Published in final edited form as:
Structure. 2008 October ; 16(10): 1555–1561. doi:10.1016/j.str.2008.07.013.

Structure of Seneca Valley Virus-001, An oncolytic picornavirus representing a new genus

Sangita Venkataraman[1], **Seshidhar P. Reddy**[2], **Jackie Loo**[1], **Neeraja Idamakanti**[2], **Paul L. Hallenbeck**[2], and **Vijay S. Reddy**[1*]

1*Department of Molecular Biology, The Scripps Research Institute, La Jolla, CA 92037*

2*Neotropix Inc., 351 Phoenixville Pike, Malvern, PA 19355*

SUMMARY

The crystal structure of Seneca Valley Virus-001, SVV-001, the representative member of a new genus "Senecavirus" is reported at 2.3Å resolution. SVV-001 is the first naturally occurring non-pathogenic picornavirus seen to mediate selective cytotoxicity towards tumor cells with neuroendocrine cancer features. The non-segmented (+) ssRNA genome of SVV-001 shares closest sequence similarity with the genomes of the members of *Cardiovirus*. The overall tertiary structure of VP1-VP4 subunits is conserved with the exception of loops, especially those of VP1 that show large deviations relative to the members of the Cardioviruses. The surface loops of VP1 and VP2 are predicted to mediate cell tropism of SVV-001. In addition, the organization of the packaged nucleic acid density indicates that certain regions of VP2 and VP4 interact closely with the packaged nucleic acid.

INTRODUCTION

Viruses have been used in the treatment of cancer from as early as 1940s with the first human clinical trial dating back to 1956 for the treatment of cervical cancer (Huebner et al., 1956). Among the new virotherapies, use of viruses that specifically infect cancer cells is in the forefront (Lin and Nemunaitis, 2004). These include the CAV21 (Au et al., 2005) developed by Virolytics under the name of CAVATAK, Reovirus (Thirukkumaran et al., 2003) based REOLYSIN developed by Oncolytics Biotech Inc, Newcastle disease virus (Fiola et al., 2006) developed by Theravir Management Ltd, Vesicular stomatitis virus (Diaz et al., 2007) developed by Onco Therapy Science and the Measles virus (Yanagi et al., 2006). A new member to join this group is the Seneca Valley Virus-001 (SVV-001).

SVV-001 is the first member of a new genus called "Senecavirus" in the family of *Picornaviridae* that is proposed to include other porcine picornaviruses that share similarity in sequence and biochemical properties with SVV-001 (Hales et al., 2008; Reddy et al., 2007). SVV-001 was serendipitously discovered as a contaminant during cultivation of PER.C6 cells, transformed fetal retinoblast cells, (Fallaux et al., 1998; Reddy et al., 2007) and is presumed to be introduced via bovine serum or porcine trypsin source. SVV-001 shows closest sequence similarity to cardioviruses among other known picornaviruses and has an infectious RNA

*To whom correspondence should be addressed, Vijay S. Reddy, Ph.D., Department of Molecular Biology, TPC-6, The Scripps Research Institute, 10550 North Torrey Pines Road, La Jolla, CA 92037, E-mail: reddyv@scripps.edu Phone: (858) 784-8191, Fax: (858) 784-8660.

genome (Genbank accession no. DQ641257) of 7310 bases that codes for four capsid proteins and seven other non-structural proteins. There are long and short UTRs at the 5' and 3' ends of the genome, respectively (Hales et al., 2008). SVV-001 does not infect humans but propagates in tumor cells showing neuroendocrine features. This property is being exploited for developing SVV-001 as an oncolytic agent against tumors such as small cell lung cancer (Reddy et al., 2007). The virus is presently being studied extensively and characterized by Neotropix under the trade name NTX-010.

This study describes the structure of SVV-001 and discusses some of the receptors on cancer cells that the virus could potentially bind to during its entry into the susceptible cells. In addition, the characteristics of the bulk organization of packaged nucleic acid visualized at 20Å resolution and its interactions with the contiguous capsid shell of SVV-001 are also examined.

RESULTS AND DISCUSSION

Structure of SVV-001

The protomer of SVV-001 is composed of four different subunits, VP1, VP2, VP3 and VP4, of lengths 265, 286, 241 and 74 residues, respectively. The overall folds of the subunits (Figure 1) are very similar to the corresponding proteins in other viruses from the *Picornaviridae* family. Similar to other Cardioviruses (Grant et al., 1992;Krishnaswamy and Rossmann, 1990;Luo et al., 1992;Luo et al., 1987), SVV-001 possesses a hydrophobic pocket without a pocket factor. However, the hydrophobic cleft in the VP1 subunit of SVV-001 is almost completely sealed off by residues W142, F182, W186, D215 and W216 from the same subunit unlike the cardioviruses and rhinoviruses (Hadfield et al., 1997;Kim et al., 1989;Verdaguer et al., 2000;Zhao et al., 1996) where the entrances to the cleft are small and big, respectively.

The reasons for the variant cell tropism of picornaviruses are owing to the composition, location, length and disposition of surface exposed loops of the capsid proteins, which are typical of individual viruses in *Picornaviridae* (Rossmann et al., 1985). In SVV-001, BC loop (residues 50–74), loop II (CD loop, residues 94–109) and FMDV loop (GH loop, residues 185–215) of VP1, “the Puff” (EF loop, residues 172–200) of VP2 and “the Knob” (residues 57–73) of the VP3 subunit are of particular importance (Figure 1) as they are more prominent in length when compared to other members of *Picornaviridae* (Filman et al., 1998; Fry et al., 2003; Grant et al., 1992; Hadfield et al., 1997; Hogle et al., 1985; Kim et al., 1989; Krishnaswamy and Rossmann, 1990; Logan et al., 1993; Luo et al., 1992; Muckelbauer et al., 1995; Rossmann et al., 1985). On the contrary, loop I (CD loop, residues 82–87 of VP1) in SVV-001 is shorter and concealed by the loops BC and II of VP1. Apart from the knob of VP3 subunit, the other loops of SVV-001 are structurally well ordered.

The capsid of SVV-001 has a maximum diameter of 325Å with a contiguous shell thickness of 25Å and surface unevenness (Figure 2a). The highest elevation (325Å in diameter) occurs close to the fivefold axis and is formed by the stacking of three loops, two from VP1 (loops BC and II) and the third from VP2 (the Puff). The knob of VP3 stands alone closest to the threefold axis. The accessible surface area of the residues of the various loops of the three subunits, as calculated using VIPERdb (Shepherd et al., 2006), suggests that the loops II of VP1 and the knob of VP3 have the highest effective solvent accessible surface area (SASA) of ~7000 $Å^2$. The Puff of the VP2 subunit has an effective SASA of ~6000 $Å^2$. As oppose to the members of Rhinovirus family that display more prominent VP2 loops and smaller VP1 loops, the members of Cardiovirus have prominent loops of both VP1 and VP2. However, the lengths and disposition of these loops in SVV-001 and the other cardioviruses leads to varied surface features and the filling up of the canyon. Instead of the canyon, SVV-001 and the members of *Cardioviridae* (Figure 2b) show a sharp pit.

Analysis of the RMSDs of the main chain C α atoms of the protomer of SVV-001 with other representative members of *Picornaviridae* shows a maximum (1.4 Å, number of aligned residues ~500) and minimum (1.2 Å, number of aligned residues ~600) deviation with the members of Rhinovirus (Hadfield et al., 1997; Kim et al., 1989; Verdaguer et al., 2000; Zhao et al., 1996) and Cardiovirus (Grant et al., 1992; Krishnaswamy and Rossmann, 1990; Luo et al., 1992), respectively. In accordance with the structural similarity, SVV-001 shows maximum (~42%) and minimum (~30%) sequence identity with Mengo Encephalomyocarditis Virus (MEV) and Human Rhinovirus (HRV) 16, respectively. Figure 2, panels c, d and e show the superposition of the subunits of MEV onto corresponding subunits of SVV-001. Individually, the VP1 and VP2 subunits of SVV-001 show maximum and minimum structural variation, respectively, with the other members of *Picornaviridae*.

Nucleic acid arrangement

A low resolution (~20 Å) map of SVV-001 showed the arrangement of nucleic acid inside the capsid shell, visualized using x-ray crystallography for the first time for any picornavirus. The bulk nucleic acid organization in SVV-001 seems to be continuously in contact with the inner surface of the capsid with more prominent contacts near the icosahedral twofold axes beneath two VP2 subunits (Figure 3). There is an innermost compact sphere of density at the center of the viral capsid surrounded by a few discontinuous isolated densities. Closest to the capsid layer is a more continuous shell of RNA density that interacts with residues 43–45, 57–59 of VP2 and 38–40 of VP4 subunits and could potentially play a role as a scaffold for capsid assembly and architecture. It is possible that similar nucleic acid organization may also be present in other picornaviruses.

Putative receptors of SVV-001

Though there are receptors known for many picornaviruses (Rossmann et al., 2002), receptor (s) for Senecaviruses is yet to be determined. Since SVV-001 is known to target cells with neuroendocrine tumor features, it is possible that the cell tropism of SVV-001 might be governed by binding to receptors expressed on such tumor cells. A few that have been suggested include markers like gastrin-releasing peptide receptors, synaptophysin, neuron-specific enolase, and CD56 (Wadhwa et al., 2007). However, no structural evidence could be established for the binding of SVV-001 to any of these receptors. Nevertheless, the outer capsid features of SVV-001 were analyzed to gain insights into other possible receptors to which it might bind (Figures 4a and 4b). Of these were the α_v integrins, which are recognized by the RGD motif in FMDV (Logan et al., 1993). It is known that the KGD motif mimics RGD in many cases (Reiss et al., 2006; Xinjie et al., 2006). Although the motif, KGD, does not occur on the surface of SVV-001 capsids, but it's reverse motif, DGK (residue 148–150), is found in the VP2 subunit of SVV-001. The main chain conformation of RGD bound to integrin molecule in a RGD-integrin complex (Xiong et al., 2002) matches very well with the main chain conformation of the DGK motif of SVV-001 (Figure 4c). Furthermore, the DGK motif is exposed on the surface of SVV-001 and is located in the canyon formed by the VP1/2 loops and the puff of VP2. So it is likely that the DGK motif might play an important role in recognizing integrin receptors on the cell surfaces. In addition to the DGK motif, another integrin binding motif, LDV (residues 143–145 of VP2), also exists on the surface of SVV-001 capsids. This motif is known to bind to specific $\alpha_1\beta_4$ integrins expressed on small cell lung cancer cells (Tselepis et al., 1997). However, the LDV motif is not exposed on the surface and lies in a depression that is immediately next to "the puff" of VP2 subunit and is less accessible (Figure 4d). However, it is not unlikely that local conformational changes could expose this motif and aid in receptor binding. Since DGK and LDV motifs are structurally proximal (Figure 4b), it is possible that they can be jointly involved in binding to integrins on the cell surface.

Another receptor that SVV-001 could bind to is the low-density lipoprotein (LDL) receptor. Essentially the N-terminal extracellular region of LDL receptor (LDLR) is the one that is recognized by viruses. The HRV2 structure (Verdaguer et al., 2004) complexed with a fragment of the receptor suggests that three residues interact with the receptor of which K224 of VP1 is most crucial and conserved in all minor group members (e.g., HRV1a). The structural superposition of SVV-001 onto HRV2-LDLR showed that a highly exposed lysine (K228) of VP1 in SVV-001 nearly overlaps with the conserved lysine, K224 of HRV2 that is known to be involved in crucial interactions with the LDLR. Except for this lysine the other proximal residues are variable among the members of minor group rhinoviruses that bind to the LDL receptor. The K228 of SVV-001 is exposed with an effective SASA of 4500 $Å^2$ and could play a role in binding to LDLR suggesting that the LDLR is another plausible receptor for SVV-001 (Figure 4e).

Additionally, structural comparison of SVV-001 with MEV (Krishnaswamy and Rossmann, 1990; Luo et al., 1987) shows that there is no corresponding lysine for K229 in the MEV structure. In fact the loop (HI), which harbors K229 in SVV-001 is much shorter in MEV and takes a different path. Although, on the whole, the SVV-001 structure is closest to MEV, it resembles rather well locally with the LDL-binding region of HRV2. However, the LDV motif seen in SVV-001 is also present in MEV, but absent in HRV2. Interestingly, the LDV motif in MEV is surface accessible, however, the involvement of this motif in receptor binding has not been investigated for MEV. The DGK motif seen in SVV-001 is not present in MEV.

EXPERIMENTAL PROCEDURES

The SVV-001 was crystallized in a R3 space group with unit cell dimensions **a**=**b**=311.5Å, **c**=1526.4Å, α=β=90°, γ=120° and it's structure was determined at 2.3Å resolution by molecular replacement using MEV capsid as the model (Venkataraman et al., 2008). The unit cell of SVV-001 is unusual because of a long **c**-axis (1526Å) that is nearly 4.9 times the lengths of **a** or **b** axis (311Å) and hence accommodates six virus particles. Two sets of 20mers contributed by two distinct virus particles located at (0., 0., 0.) and (0.333, 0.666, 0.166) occupy the crystallographic asymmetric unit. The orientation of the two distinct particles were determined using the program GLRF (Tong and Rossmann, 1990) and the particle positions were determined using the program Phaser (Read, 2001; Storoni et al., 2004). The initial phase extention and NCS averaging using RAVE (Kleywegt and Jones, 1994) and CCP4 suite of programs (CCP4, 1994) resulted in readily interpretable maps at 2.3Å with a final real space R-factor of 0.23 and correlation coefficient of 0.93.

The final model was built manually into the electron density map contoured at 1.2σ using the program O (Jones et al., 1991). The structure was refined using the program CNS (Brunger et al., 1998) imposing (strict) 40-fold non-crystallographic symmetry (NCS) constraints. Water molecules were picked initially using the program CNS and later manually from once averaged *Fo-Fc* map contoured at 2.5σ. A low-resolution (100-20Å) vector difference map was calculated by subtracting model amplitude and phases from the Fobs and phase-refined phases to visualize the bulk nucleic acid density. The final refinement statistics are shown in Table1. The coordinates and structure factors were deposited in RCSB with a PDB-ID of 3CJI.

Model quality was analyzed using PROCHECK (Laskowski et al., 1993) and Stride (Heinig and Frishman, 2004) was used for the assignment of secondary structures. TOP3d from CCP4 suite of programs and ALIGN (Cohen, 1997) were used for structure alignment. Pymol (http://www.pymol.org), Chimera (Pettersen et al., 2004) and VMD (Humphrey et al., 1996) were used for structure visualization, analysis and generation of figures. VIPERdb analysis (Shepherd et al., 2006) was employed to estimate buried and accessible surface areas and

association energies. Intra/Intersubunit contacts, average B, and individual accessible surface area were calculated using CCP4 suite of programs (CCP4, 1994).

ACKNOWLEDGEMENTS

We are extremely grateful for the assistance and help of the staff at the BIOCARS facility Drs. Vukica Srajer, Reinhard Pahl, and Spencer Anderson in setting up experiment under the BSL2 conditions. This work was partially supported by the NIH grant R56 AI070771 to V.S.R. Partial salary support to V.S.R. by NIH Research Resource Multi Scale Modeling Tools for Structural Biology (MMTSB), RR12255 is acknowledged.

References

Au GG, Lindberg AM, Barry RD, Shafren DR. Oncolysis of vascular malignant human melanoma tumors by Coxsackievirus A21. International journal of oncology 2005;26:1471–1476. [PubMed: 15870858]

Bajaj C, Djeu P, Thane A, Siddavanahalli V. Interactive visual exploration of large flexible multi-component molecular complexes. Proc. of the Annual IEEEE Visualization Conference 2004:243–250.

Brunger AT, Adams PD, Clore GM, DeLano WL, Gros P, Grosse-Kunstleve RW, Jiang JS, Kuszewski J, Nilges M, Pannu NS, et al. Crystallography & NMR system: A new software suite for macromolecular structure determination. Acta crystallographica 1998;D54:905–921.

CCP4. The CCP4 suite: programs for protein crystallography. Acta crystallographica 1994;D50:760–763.

Cohen GE. ALIGN: a program to superimpose protein coordinates, accounting for insertions and deletions. Journal of Applied Crystallography 1997;30:1160–1161.

Diaz RM, Galivo F, Kottke T, Wongthida P, Qiao J, Thompson J, Valdes M, Barber G, Vile RG. Oncolytic immunovirotherapy for melanoma using vesicular stomatitis virus. Cancer research 2007;67:2840–2848. [PubMed: 17363607]

Fallaux FJ, Bout A, van der Velde I, van den Wollenberg DJ, Hehir KM, Keegan J, Auger C, Cramer SJ, van Ormondt H, van der Eb AJ, et al. New helper cells and matched early region 1-deleted adenovirus vectors prevent generation of replication-competent adenoviruses. Human gene therapy 1998;9:1909–1917. [PubMed: 9741429]

Filman DJ, Wien MW, Cunningham JA, Bergelson JM, Hogle JM. Structure determination of echovirus 1. Acta crystallographica 1998;D54:1261–1272.

Fiola C, Peeters B, Fournier P, Arnold A, Bucur M, Schirrmacher V. Tumor selective replication of Newcastle disease virus: association with defects of tumor cells in antiviral defence. International journal of cancer 2006;119:328–338.

Fry EE, Knowles NJ, Newman JW, Wilsden G, Rao Z, King AM, Stuart DI. Crystal structure of Swine vesicular disease virus and implications for host adaptation. Journal of virology 2003;77:5475–5486. [PubMed: 12692248]

Grant RA, Filman DJ, Fujinami RS, Icenogle JP, Hogle JM. Three-dimensional structure of Theiler virus. Proceedings of the National Academy of Sciences of the United States of America 1992;89:2061–2065. [PubMed: 1549565]

Hadfield AT, Lee W, Zhao R, Oliveira MA, Minor I, Rueckert RR, Rossmann MG. The refined structure of human rhinovirus 16 at 2.15 A resolution: implications for the viral life cycle. Structure 1997;5:427–441. [PubMed: 9083115]

Hales LM, Knowles NJ, Reddy PS, Xu L, Hay C, Hallenbeck PL. Complete genome sequence analysis of Seneca Valley virus-001, a novel oncolytic picornavirus. The Journal of general virology 2008;89:1265–1275. [PubMed: 18420805]

Heinig M, Frishman D. STRIDE: a web server for secondary structure assignment from known atomic coordinates of proteins. Nucleic acids research 2004;32:W500–W502. [PubMed: 15215436]

Hogle JM, Chow M, Filman DJ. Three-dimensional structure of poliovirus at 2.9 A resolution. Science 1985;229:1358–1365. [PubMed: 2994218]

Huebner RJ, Rowe WP, Schatten WE, Smith RR, Thomas LB. Studies on the use of viruses in the treatment of carcinoma of the cervix. Cancer 1986;9:1211–1218. [PubMed: 13383455]

Humphrey W, Dalke A, Schulten K. VMD: visual molecular dynamics. Journal of molecular graphics 1996;14:33–38. [PubMed: 8744570]

Jones TA, Zou JY, Cowan SW, Kjeldgaard M. Improved methods for building protein models in electron density maps and the location of errors in these models. Acta crystallographica 1991;A47(Pt 2):110–119. [PubMed: 2025413]

Kim SS, Smith TJ, Chapman MS, Rossmann MC, Pevear DC, Dutko FJ, Felock PJ, Diana GD, McKinlay MA. Crystal structure of human rhinovirus serotype 1A (HRV1A). Journal of molecular biology 1989;210:91–111. [PubMed: 2555523]

Kleywegt GJ, Jones TA. From First Map to Final Model. CCP4 Proceedings 1994:59–66.

Krishnaswamy S, Rossmann MG. Structural refinement and analysis of Mengo virus. Journal of molecular biology 1990;211:803–844. [PubMed: 2156078]

Laskowski RA, McArthur MW, Moss DS, Thornton JM. PROCHECK: a program to check the stereochemical quality of protein structures. Journal of Applied Crystallography 1993;26:283–291.

Lin E, Nemunaitis J. Oncolytic viral therapies. Cancer gene therapy 2004;11:643–664. [PubMed: 15286681]

Logan D, Abu-Ghazaleh R, Blakemore W, Curry S, Jackson T, King A, Lea S, Lewis R, Newman J, Parry N, et al. Structure of a major immunogenic site on foot-and-mouth disease virus. Nature 1993;362:566–568. [PubMed: 8385272]

Luo M, He C, Toth KS, Zhang CX, Lipton HL. Three-dimensional structure of Theiler murine encephalomyelitis virus (BeAn strain). Proceedings of the National Academy of Sciences of the United States of America 1992;89:2409–2413. [PubMed: 1312722]

Luo M, Vriend G, Kamer G, Minor I, Arnold E, Rossmann MG, Boege U, Scraba DG, Duke GM, Palmenberg AC. The atomic structure of Mengo virus at 3.0 A resolution. Science 1987;235:182–191. [PubMed: 3026048]

Muckelbauer JK, Kremer M, Minor I, Tong L, Zlotnick A, Johnson JE, Rossmann MG. Structure determination of coxsackievirus B3 to 3.5 A resolution. Acta crystallographica 1995;D51:871–887.

Pettersen EF, Goddard TD, Huang CC, Couch GS, Greenblatt DM, Meng EC, Ferrin TE. UCSF Chimera--a visualization system for exploratory research and analysis. Journal of computational chemistry 2004;25:1605–1612. [PubMed: 15264254]

Read RJ. Pushing the boundaries of molecular replacement with maximum likelihood. Acta crystallographica 2001;D57:1373–1382.

Reddy PS, Burroughs KD, Hales LM, Ganesh S, Jones BH, Idamakanti N, Hay C, Li SS, Skele KL, Vasko AJ, et al. Seneca Valley virus, a systemically deliverable oncolytic picornavirus, and the treatment of neuroendocrine cancers. Journal of the National Cancer Institute 2007;99:1623–1633. [PubMed: 17971529]

Reiss S, Sieber M, Oberle V, Wentzel A, Spangenberg P, Claus R, Kolmar H, Losche W. Inhibition of platelet aggregation by grafting RGD and KGD sequences on the structural scaffold of small disulfide-rich proteins. Platelets 2006;17:153–157. [PubMed: 16702041]

Rossmann MG, Arnold E, Erickson JW, Frankenberger EA, Griffith JP, Hecht HJ, Johnson JE, Kamer G, Luo M, Mosser AG, et al. Structure of a human common cold virus and functional relationship to other picornaviruses. Nature 1985;317:145–153. [PubMed: 2993920]

Rossmann MG, He Y, Kuhn RJ. Picornavirus-receptor interactions. Trends in microbiology 2002;10:324–331. [PubMed: 12110211]

Shepherd CM, Borelli IA, Lander G, Natarajan P, Siddavanahalli V, Bajaj C, Johnson JE, Brooks CL 3rd, Reddy VS. VIPERdb: a relational database for structural virology. Nucleic acids research 2006;34:D386–D389. [PubMed: 16381893]

Storoni LC, McCoy AJ, Read RJ. Likelihood-enhanced fast rotation functions. Acta crystallographica 2004;D60:432–438.

Thirukkumaran CM, Luider JM, Stewart DA, Cheng T, Lupichuk SM, Nodwell MJ, Russell JA, Auer IA, Morris DG. Reovirus oncolysis as a novel purging strategy for autologous stem cell transplantation. Blood 2003;102:377–387. [PubMed: 12637331]

Tong LA, Rossmann MG. The locked rotation function. Acta crystallographica 1990;46(Pt 10):783–792. [PubMed: 2174243]

Tselepis VH, Green LJ, Humphries MJ. An RGD to LDV motif conversion within the disintegrin kistrin generates an integrin antagonist that retains potency but exhibits altered receptor specificity. Evidence for a functional equivalence of acidic integrin-binding motifs. The Journal of biological chemistry 1997;272:21341–21348. [PubMed: 9261147]

Venkataraman S, Reddy SP, Loo J, Idamakanti N, Hallenbeck PL, Reddy VS. Crystallization and preliminary X-ray diffraction studies of Seneca Valley Virus-001, a new member of the Picornaviridae family. Acta crystallographica 2008;F64:293–296. [PubMed: 18391430]

Verdaguer N, Blaas D, Fita I. Structure of human rhinovirus serotype 2 (HRV2). Journal of molecular biology 2000;300:1179–1194. [PubMed: 10903863]

Verdaguer N, Fita I, Reithmayer M, Moser R, Blaas D. X-ray structure of a minor group human rhinovirus bound to a fragment of its cellular receptor protein. Nature structural & molecular biology 2004;11:429–434.

Wadhwa L, Hurwitz MY, Chevez-Barrios P, Hurwitz RL. Treatment of invasive retinoblastoma in a murine model using an oncolytic picornavirus. Cancer research 2007;67:10653–10656. [PubMed: 18006805]

Xinjie L, Joanna D, Dong L, Min X, Beth W, Dazhuang S, Yingqing S, Mike S, Vijay K. The Effect of the Single Substitution of Arginine within the RGD Tripeptide Motif of a Modified Neurotoxin Dendroaspin on Its Activity of Platelet Aggregation and Cell Adhesion. Cell Communication and Adhesion 2006;13:171–183. [PubMed: 16798616]

Xiong JP, Stehle T, Zhang R, Joachimiak A, Frech M, Goodman SL, Arnaout MA. Crystal structure of the extracellular segment of integrin alpha Vbeta3 in complex with an Arg-Gly-Asp ligand. Science 2002;296:151–155. [PubMed: 11884718]

Yanagi Y, Takeda M, Ohno S. Measles virus: cellular receptors, tropism and pathogenesis. The Journal of general virology 2006;87:2767–2779. [PubMed: 16963735]

Zhao R, Pevear DC, Kremer MJ, Giranda VL, Kofron JA, Kuhn RJ, Rossmann MG. Human rhinovirus 3 at 3.0 A resolution. Structure 1996;4:1205–1220. [PubMed: 8939746]

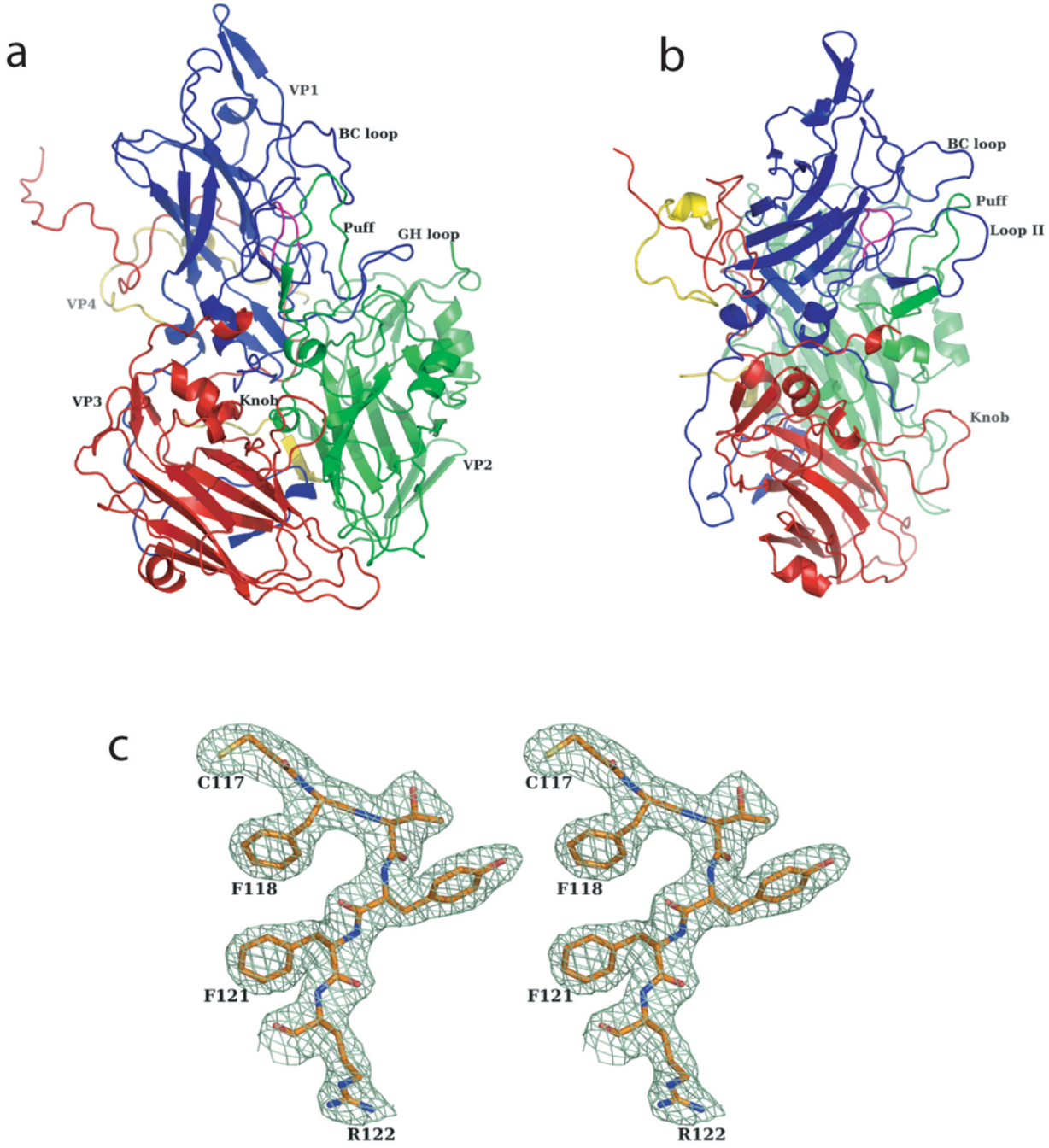

Figure 1.

Protomer structure and the quality of the electron density map of SVV-001. Ribbon diagrams of SVV-001 protomer, (a) front view and (b) a side view, highlighting the different subunits and the prominent surface loops. VP1, VP2, VP3 and VP4 subunits are shown in blue, green, red and yellow respectively. (c) Stereo diagram showing the quality of the NCS averaged electron density map at 2.3Å resolution, contoured at 1.2σ.

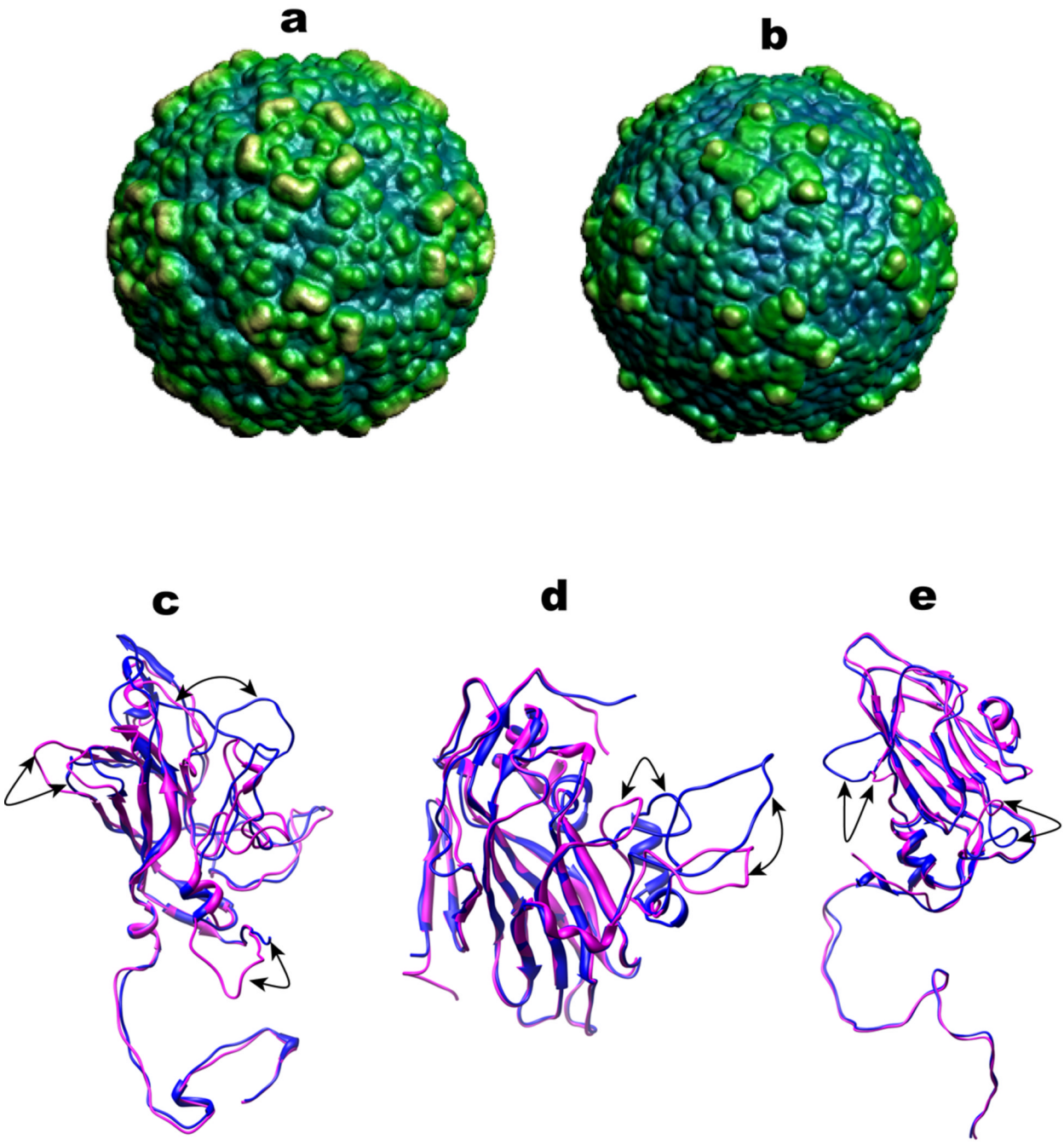

Figure 2.

Structural comparison of SVV-001 and MEV capsids: (a) Surface rendered illustrations of (a) SVV-001 and (b) MEV capsid highlighting the differences of their surfaces, generated using the program TexMol (Bajaj et al., 2004). A coloring scheme of blue to yellow was used as a function of the distance from the centre of the virus. The blue regions represent the depressions while the yellow regions represent the elevations on the surface. Ribbon diagrams of the superposition of (c) VP1, (d) VP2 and (e) VP3 subunits of MEV (Magenta) onto the corresponding subunits of SVV-001 (Blue). Corresponding loops showing maximum structural differences are highlighted by arrows.

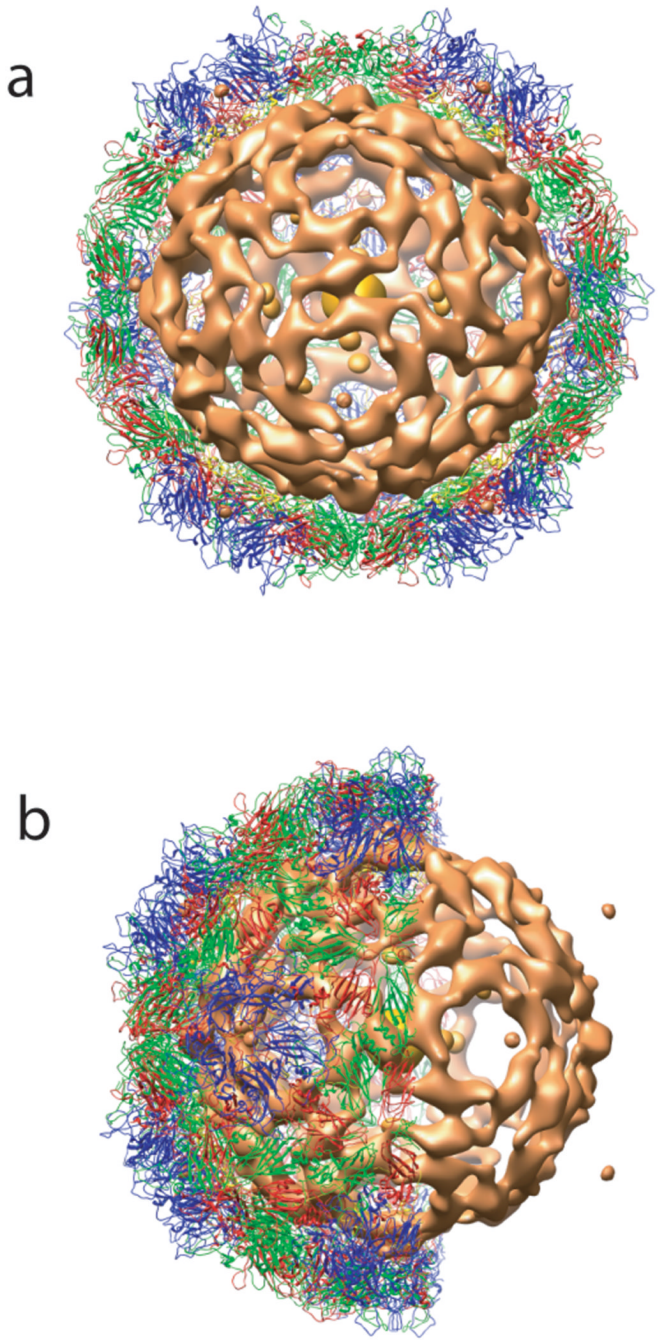

Figure 3.
An illustration of nucleic acid organization in SVV-001 at 20Å resolution. a) A view down the particle 2-fold axis showing the bulk RNA density (orange) and part of the protein shell. b) A side view of the same.

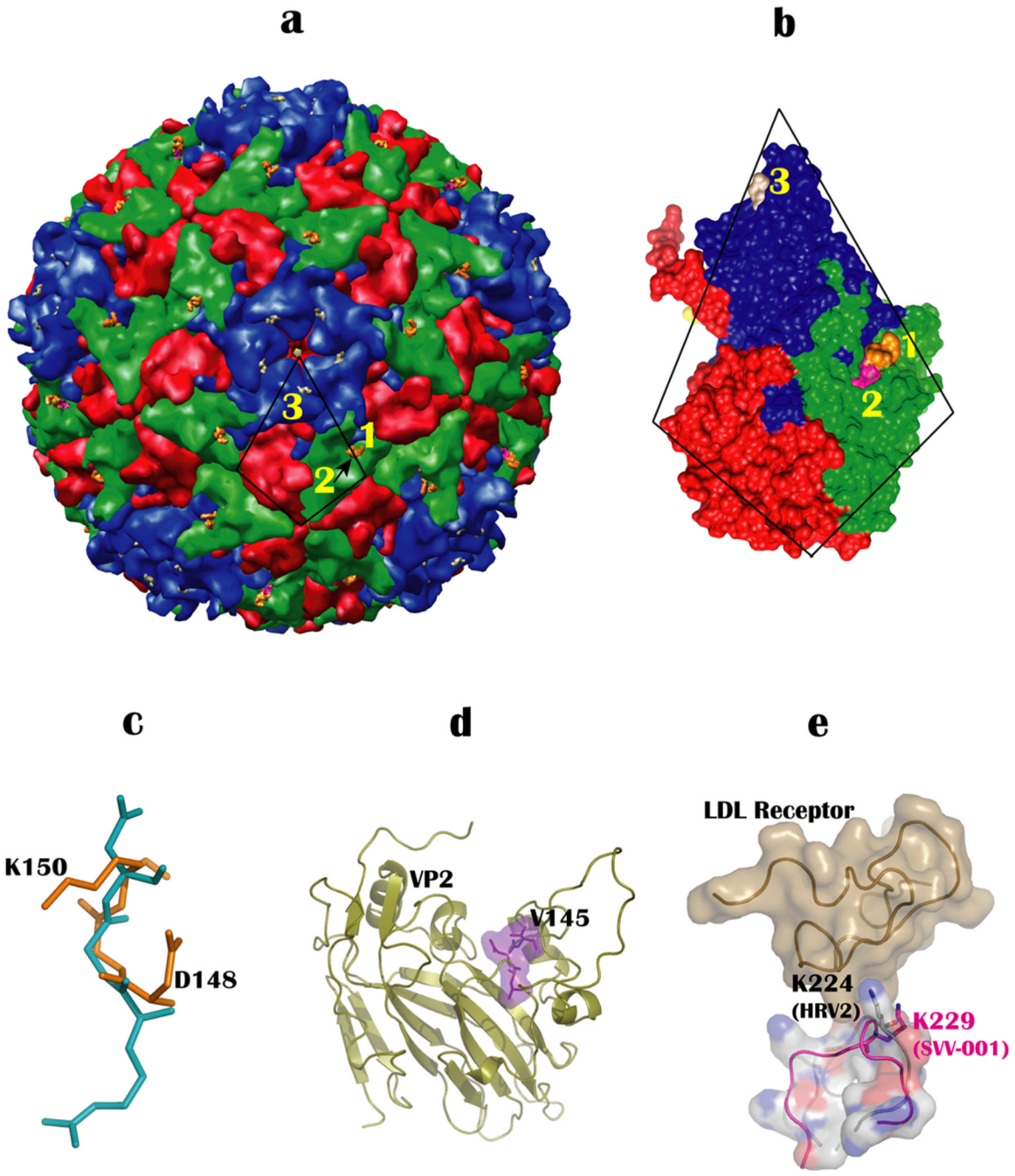

Figure 4.

Locations of putative receptor binding sites on SVV-001. (a) Positions of major receptor binding motifs on the surface of SVV-001. Sites numbered 1 and 2 indicate the locations of the DGK and the LDV motif while K229 is numbered 3. The LDV motif (site 2) is hidden under the DGK motif (site 1) and is indicated by an arrow. The icosahedral asymmetric unit comprising VP1-4 is indicated by a trapezoid. (b) Enlarged view of the icosahedral asymmetric unit oriented to highlight the positions of DGK, LDV and K229. (c) The superposition of DGK motif (gold) on the RGD motif (cyan). (c) Location of the LDV motif, shown as purple surface and stick diagram, in the VP2 subunit. (d) Structural superposition of loop containing K229 (VP1) of SVV-001 (pink) onto LDL binding loop of HRV2. The structural proximity of K229

of SVV-001 with the critical residue, K224 of HRV2 in the HRV2-LDL receptor (baize colored surface) complex, indicates that it might play a similar role in binding to the LDL receptor in SVV-001.

Table 1

Data refinement statistics

Parameters	Data
Space group	R3
Unit cell dimensions	**a**=**b**=311.5Å, **c**=1526.4Å, α=β=90°, γ=120°
Resolution range (Å)	100 – 2.3 (2.4 – 2.3)[§]
R factor / free R (%)	25.8(37.7) / 26.0(37.7)
No. of Protein atoms/asymmetric unit	6253
No. of Solvent/asymmetric unit	267
RMSD bond (Å)	0.006
RMSD angles (°)	1.4
Average B factor (main-chain) (Å^2)	41.0
Ramachandran statistics	
Most Favored region (%)	87.2
Additionally allowed region (%)	12.1
Generously allowed region (%)	0.4
Disallowed region (%)	0.3

[*] $R_{merge} = \sum hkl|I-\langle I\rangle|/\sum I$

[§] Data in parenthesis refer to the last resolution shell